Innovative Metallized Formulations for Solid Rocket Propulsion

Luigi T DeLUCA, Luciano GALFETTI, Filippo MAGGI, Giovanni COLOMBO, Alice REINA, Stefano DOSSI, Daniele CONSONNI, Melissa BRAMBILLA

（SPLab, Dipartimento di Ingegneria Aerospaziale, Politecnico di Milano, I-20156 Milan, Italy）

Abstract：Several metallized solid rocket propellants, AP/Metal/HTPB in the ratio 68/18/14, were experimentally analyzed at the Space Propulsion Laboratory of Politecnico di Milano. Effects of the metals (micrometric and nanometric Al, B, Mg, and a variety of dual metals) on the performance of the propellant were studied and contrasted to a conventional micrometric aluminum (30 μm average grain size) taken as reference. It is shown that the propellant microstructure plays a fundamental role in controlling the critical aggregation/agglomeration phenomena occurring below and near the burning surface. Two specific effects of microstructure in terms of steady burning rate and average agglomerate size are illustrated.

Key words：solid propellants; metal powders; combustion; specific impulse; burning rate; agglomeration

1 Introduction

High-energy solid propellant formulations, based on Ammonium Perchlorate (AP) and Aluminum (Al) particles bound by an inert binder, Hydroxyl-Terminated PolyButadiene (HTPB), play an essential role in primary propulsion for space exploration. Investigations were carried out all around the world during the last decades to improve the delivered performance of AP/Al/HTPB compositions currently used for space launchers[1,2,3]. The crucial function of metal agglomeration was clarified and the need was subsequently underlined of improving combustion efficiency and two-phase (2P) losses associated with supersonic expansion in gasdynamic nozzles[4,5,6].

But the endless quest for better propulsive systems prompts for higher ballistic performance while maintaining acceptable levels of mechanical properties, aging characteristics, cost, and processability. Performance of solid rocket propellants can be increased in terms of gravimetric (I_s) as well as volumetric specific impulse (I_v) by resorting to energetic additives which increase energy content and compound density. Thus, international research projects currently aim at developing and testing innovative metallized fuels, allowing at the same time an increase of density and delivered specific impulse, by enhancing the ideal performance and/or its efficiency.

The submitted paper expands on previous investigations by this research group[7,8,9,10,11] and points out new directions using inert binders loaded with high-energy fuels consisting of various metal mixtures for solid propellants (AP/HTPB-based) typically used in rocket propulsion. Numerous formulations were experimentally analyzed at the Space Propulsion Laboratory (SPLab) of Politecnico di Milano and contrasted to the corresponding formulations using a conventional propulsion grade micrometric aluminum (30 μm average grain size)

taken as reference. Steady burning rates and the associated flame structure were studied by a variety of experimental techniques ranging from high-speed and high-resolution digital video recording to chemo-physical analyses of the solid combustion residues.

For reader's convenience, the following technical jargon is implemented in this paper. The word agglomeration is reserved to spherical drops of liquid metal in combustion with an oxide cap, while the word aggregation is reserved to partially oxidized objects of irregular shape typically seen as precursors of agglomeration. Agglomeration always implies a loss of the initial particle individuality, while aggregation may keep some remnant of the initial particle individuality. As defined, both agglomeration and aggregation are typically manifested by Aluminum burning. The word cohesion (or adhesion) is reserved to "a portion of a substance cleaving together in a thick nondescript mass", while coagulation is reserved to a "viscous lump of a portion of liquid" (from Merriam-Webster Dictionary).

2 Ingredients and Propellant Formulations

The composite solid rocket propellant taken as baseline is an AP/Metal/HTPB formulation in the mass ratios 68/18/14. A laboratory reproduction of a flight certified Al-based formulation, containing as metal only propulsion grade Al (30 μm average grain size), was taken as a suitable reference. As seen respectively in Table 1 and Table 2, the oxidizer is a bimodal AP blend while the binder is a standard HTPB R-45. Except where otherwise stated, all propellants were manufactured, processed, and tested at SPLab of Politecnico di Milano under identical conditions and using identical procedures.

Table 1 Standard solid propellant composition for all tested formulations

component	mass fraction/%
AP (160 − 200 μm)	58.00
AP (5 − 10 μm)	10.00
metal fuel powder	18.00
binder	14.00

Table 2　Standard binder composition for all tested formulations

component	mass fraction/%
HTPB R-45	79.21
IsoPhorone Di-Isocyanate（IPDI）	7.68
DiOctyl Adipate（DOA）	13.11

2.1　Tested Metallic Ingredients

The characterization of the metal powders was carried out by BET（Brunauer-Emmett-Teller）, XPS（X-ray Photoelectron Spectroscopy）, XRD（X-Ray Diffraction）, SEM（Scanning Electron Microscopy）, TEM（Transmission Electron Microscopy）, and Malvern Mastersizer 2000 equipped with a Scirocco unit for dry analyses.

The BET surface of the Al-05a（30 μm）taken as industrial reference was measured as $0.1\ m^2 \cdot g^{-1}$, while for Al-06（50 μm）flakes it was found $< 0.1\ m^2 \cdot g^{-1}$. For both micrometric Aluminum（μAl）active Al content is around 99%.

2.1.1　nAl

Two nano-sized Aluminum（nAl）powders known as Alex^{TM}, with nominal size of 100 and 50 nm, were investigated[12]; see respectively Table 3 and Table 4. Both of them were produced by Explosion of Electric Wire（EEW）technique and then properly coated（series 07 and 13）. Industrial powders are typically passivated in a controlled slow dry air stream. An alternative consists in coating already-air-passivated（APS）nAl at laboratory scale. For all nAl powders, the much larger BET（by two orders of magnitude）with respect to micrometric Al assures a substantially increased reactivity, in spite of the limited active Al content（at most 90%）.

Table 3　BET specific surface area and active Al content results for 100 nm samples

properties	BET/$m^2 \cdot g^{-1}$	active Al/%
ALEX^{TM}-01i	11.8	89
L-ALEX$_{APS}$-07d	9.1	70
ALEX^{TM}-13d	6.9	78

Table 4　BET specific surface area and active Al content results for 50 nm samples

properties	BET/$m^2 \cdot g^{-1}$	active Al/%
ALEX^{TM}-01h	15.7	90
L-ALEX$_{NPS}$-07c	11.3	89

SEM and TEM images show almost spherical particles; the flake-shaped structures recognizable in some images may be indicative of some original aggregation processes（cohesion）between particles, probably due to the mechanisms of metal explosion and aerodynamics of particles in the EEW machine. During analyses of fatty acid-coated already passivated nAl particles（L-ALEX$_{APS}$, whereas L-ALEX$_{NPS}$ indicates the fatty acid-coated non passivated particles）, decomposition of the subtle organic layer surrounding the metal core of particle could be observed due to the incident beam energy. According to XRD data, peaks of Al are the only recognizable phase of the diffraction pattern for all samples, due to the very thin

coating layer surrounding Al particles, irrespective of whether coated or uncoated nAl particles are examined.

2.1.2　Mg$_x$B$_y$

The examined Mg$_x$B$_y$ particles produced by MACH I are characterized by a different fraction of Mg coating ranging from 10% to 60% and by a boron purity of either 90%（with the remaining material detected by XPS surface analysis to be mainly Aluminum）or 95%（with the remaining material detected by XPS surface analysis to be mainly Fluorine）. All of the tested Mg$_x$B$_y$ powders are listed in Table 5, with the corresponding BET specific surface when available.

Table 5　Tested Mg$_x$B$_y$ composite metal powders

powder label	B purity/%	Mg mass fraction/%	BET/$m^2 \cdot g^{-1}$
B90	90 – 92	0	18.1
B95	95 – 97	0	13.0
Mg15B85a	90 – 92	15	NAv
Mg20B80a	90 – 92	20	10.5
Mg25B75a	90 – 92	25	NAv
Mg10B90b	95 – 97	10	NAv
Mg20B80b	95 – 97	20	6.8
Mg60B40b	95 – 97	60	NAv

Note: a is Boron 90% purity, b is Boron 95% purity, NAv = Not Available.

Visual inspections of the collected SEM images of the tested metal powders provided the following general trends:

＊ Mg$_x$B$_y$ powders appear larger than the corresponding pure B powders;

＊ 95% purity B powders appear larger than the corresponding 90% purity B powders.

In addition, all of the tested B powders present an irregular shape differently from the near spherical micrometric Al used as a reference metal fuel. B powders present fine particles with no significant cohesion; Mg$_x$B$_y$ powders feature monomodal distributions with typically $d_{43} \approx 5$ μm, with the exception of Mg60B40（$d_{43} = 20.9$ μm）. While Mg$_x$B$_y$ with 90% B purity presents no significant cohesion, Mg$_x$B$_y$ with 95% B purity may occasionally display visible clots.

Particle size distributions obtained at SPLab by the Malvern Mastersizer 2000, dry unit（Scirocco）, are reported in Figure 1.
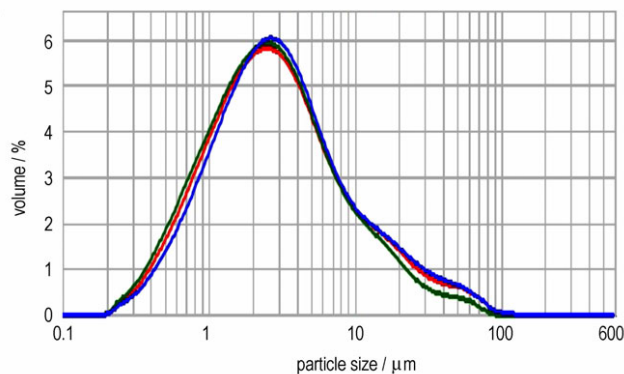
Fig.1　Particle size distribution for carefully preserved Mg$_x$B$_y$ powders. Each curve represents the mean of 4 measures. Red curve: Mg15B85a; green curve: Mg20B80a; blue curve: Mg25B75a.

Results point out that the tested metal powders tend to pack and stick together into clots. This behavior is visible when the sample is handled at normal ambient temperature and moisture. The packs are easily removed by raising the shear stresses above some threshold value. This trend to pack and stick together increases with time, if no proper care is taken during powder storage.

2.2 Tested Solid Rocket Propellants

2.2.1 Formulation

In general, the fine fraction of AP was produced at SPLab through a milling and sieving process granting a $d_{43} \approx 10$ μm. Many of the propellant formulations under test are listed in Table 6. The reference baseline only contains μAl. Both nAl and Mg_xB_y powders were used to replace either totally or partly the reference μAl fuel.

2.2.2 Density

Density measurements for several of the solid propellants under test are reported in Table 7. Theoretical Maximum Density (TMD) and porosity of the manufactured compositions were also calculated. While TMD values depend only on the accuracy of the implemented dataset, the porosity values are affected by the specific manufacturing technique, which in few cases deviate from standard processing for safety or practical reasons.

Boron is not found free in nature but is available as an amorphous powder or crystalline powder under many polymorphs. Thus, data for B-loaded propellants are respectively denoted by the label "am" and "cr" according to the amorphous or crystalline nature of Boron.

Table 6 Formulations of selected tested metallized solid propellants (mass fractions)

propellant label	AP 200 μm/%	AP < 20 μm/%	HTPB/%	Tot Metal/%	Metal	μAl/%	Metal + μAl/%
P-18Al Baseline	58	10	14	18	–	18	0 +18
P-18B90	58	10	14	18	B90	0.00	18 +0
P-18B95	58	10	14	18	B95	0.00	18 +0
P-18Mg	58	10	14	18	Mg	0.00	18 +0
P-18Zr	58	10	14	18	Zr	0.00	18 +0
P-18nAl 13d	58	10	14	18	nAl 13d	0.00	18 +0
P-3Mg15B85a + Al	58	10	14	18	Mg15B85a	15	3 +15
P-3Mg20B80a + Al	58	10	14	18	Mg20B80a	15	3 +15
P-3Mg25B75a + Al	58	10	14	18	Mg25B75a	15	3 +15
P-18Mg10B90b	58	10	14	18	Mg10B90b	0	18 +0
P-3Mg10B90b + Al	58	10	14	18	Mg10B90b	15	3 +15
P-18Mg60B40b	58	10	14	18	Mg60B40b	0	18 +0
P-3Mg60B40b + Al	58	10	14	18	Mg60B40b	1 5	3 +15

Note: a is Boron 90% purity; b is Boron 95% purity.

Table 7 Density of selected tested metallized solid propellants

propellant label	measured density /g·cm⁻³	TMD /g·cm⁻³	porosity /%
P-18B90	1.690 ±0.130	1.733am/1.730cr	2.5am/2.3cr
P-18B95	1.745 ±0.030	1.733am/1.730cr	−0.7am/ −0.9cr
P-18nAl 13d	1.696 ±0.005	1.761	3.69
P-3Mg15B85a + Al	1.737 ±0.008	1.754am/1.754cr	1.0am/1.0cr
P-3Mg20B80a + Al	1.703 ±0.022	1.754am/1.753cr	2.9am/2.9cr
P-3Mg25B75a + Al	1.749 ±0.014	1.753am/1.753cr	0.2am/0.2cr
P-18Mg10B90b	1.685 ±0.006	1.726am/1.723cr	2.4am/2.2cr
P-3Mg10B90b + Al	1.736 ±0.005	1.755am/1.754cr	1.1am/1.0cr
P-18Mg60B40b	1.622 ±0.005	1.690am/1.689cr	3.4am/3.9cr
P-3Mg60B40b + Al	1.683 ±0.004	1.749am/1.748cr	3.8am/3.7cr

Note: a is Boron 90% purity; b is Boron 95% purity; am is amorphous Boron; cr is crystalline Boron.

2.2.3 Microstructure and Pocket Composition

Pockets are privileged zones for the occurrence of agglomeration processes thanks to the presence of favorable conditions, such as the local high concentration of metal particles [13,14,15,16]. Pocket composition strictly depends on propellant formulation and is obtained by computing the mass ratio between metal, binder, and AP fine fraction; see Table 8. While AP coarse particles define the pocket size, all other ingredients identify the pocket composition. Thus, the pocket microstructure turns out to be a fuel rich mixture with respect to the overall propellant nominal formulation.

The pocket composition differs according to the loaded metal nature (Al, Mg, B, Zr), grain size of metal particles (μAl and nAl), and slightly also for the Mg content and purity of the original B powder. As a matter of simplicity, for B of 90% purity and 95% purity, spurious fractions of respectively 10% or 5% were conveniently approximated to Aluminum or Fluorine only.

3 Ideal Thermochemistry

Ideal thermochemical features of the tested metallized propellants were systematically analyzed by means of the NASA CEA code[17], taking into consideration both the overall propellant formulation and its associated microstructure.

3.1 Metallized Solid Rocket Propellants

This theoretical analysis was performed on AP/Metal/HTPB compositions under the following operating conditions:
* Combustion chamber pressure: 70 bar
* Nozzle area ratio $A_e/A_t = 40$
* Nozzle expansion in vacuum
* Shifting equilibrium model

The effects of the metallic ingredient addition on ideal specific impulse $I_{s,vacuum}$ as well as adiabatic flame temperature T_{flame} and CCP are seen in Table 9. A decrease of ideal gravimetric specific impulse and adiabatic flame temperature is visible, to varying extents, whenever Al is replaced by any of the tested metallic ingredients.

As shown in Table 9, under the explored operating conditions, the ideal gravimetric specific impulse decreases whenever Al is replaced, totally or partially, by B, Mg, Zr, and Mg_xB_y composite metals. Similarly, the volumetric specific impulse I_v, defined as I_v = density x I_s, decreases whenever Al (2.702 g·cm^{-3} density) is replaced, totally or partially, by B (2.340 g·cm^{-3} density if crystalline but 2.370 g·cm^{-3} if amorphous), Mg (1.738 g·cm^{-3} density), and Mg_xB_y composite metals; only Zr (6.52 g·cm^{-3} density) has a positive effect on the compound density and subsequently the volumetric specific impulse. The same negative effect takes place for the adiabatic flame temperature when Al is replaced. At the same time, however, an encouraging result is noticed in the reduction of the CCP mass at least in terms of grams of exhaust CCP per 100 g of burnt propellant. This positive effect counteracts the negative effects on ideal specific impulses and promises a good dividend on the specific impulse efficiency. This is the most relevant result from the ideal thermochemical analysis. However, it is important to remember that real gains attainable from two-phase loss reduction should be in the order of 3% of the ideal specific impulse, according to past investigations [3].

In particular, while standard aluminized compositions have 32.08 g of CCP per 100 g of burnt propellant, some of the Mg_xB_y-based composition perform as low as 3.99 g/100 g. Mole fractions follow a different trend because of the widely different molar masses of the main products; for example, boron nitride BN with 24.82 g/mol is much lighter than alumina Al_2O_3 with 101.96 g/mol. Notice that solid BN is found at the throat section for all propellants loaded with Mg_xB_y, except propellant 15% Al + 3% Mg60B40; other investigated propellants have only solid alumina as condensed product at the throat section.

Table 8 Pocket composition of selected tested metallized propellants (mass fractions relative to local composition)

propellant label	AP/%	HTPB/%	Al/%	Mg/%	B/%	Zr/%	Al^a/%	F^b/%
P-18Al	23.81	33.33	42.86	0.00	0.00	0.00	0.00	0.00
P-18B90	23.81	33.33	0.00	0.00	38.57	0.00	4.29	0.00
P-18B95	23.81	33.33	0.00	0.00	40.72	0.00	0.00	2.14
P-18Mg	23.81	33.33	0.00	42.86	0.00	0.00	0.00	0.00
P-18Zr	23.81	33.33	0.00	0.00	0.00	42.86	0.00	0.00
P-3Mg15B85a + Al	23.81	33.33	35.71	1.07	5.46	0.00	0.61	0.00
P-3Mg20B80a + Al	23.81	33.33	35.71	1.43	5.14	0.00	0.57	0.00
P-3Mg25B75a + Al	23.81	33.33	35.71	1.79	4.82	0.00	0.54	0.00
P-18Mg10B90b	23.81	33.33	0.00	4.29	36.65	0.00	0.00	1.93
P-3Mg10B90b + Al	23.81	33.33	35.71	0.72	6.11	0.00	0.00	0.32
P-18Mg15B85b	23.81	33.33	0.00	6.43	34.61	0.00	0.00	1.82
P-18Mg20B80b	23.81	33.33	0.00	8.57	32.57	0.00	0.00	1.71
P-18Mg25B75b	23.81	33.33	0.00	10.72	30.54	0.00	0.00	1.61
P-18Mg60B40b	23.81	33.33	0.00	25.72	16.29	0.00	0.00	0.86
P-3Mg60B40b + Al	23.81	33.33	35.71	4.29	2.72	0.00	0.00	0.14

Note: a is Boron 90% purity remaining being Aluminum; b is Boron 95% purity remaining being Fluorine.

Table 9 Specific impulse in vacuum, adiabatic flame temperature, molar mass and condensed combustion products. CCP data refer to nozzle throat section. Molar mass is for gas only combustion products

propellant	I_{sp_vacuum}/(Ns/kg)	T_{flame}/K	molar mass/(g/mol)	CCP type	CCP/(g/100g)	CCP/(mol/100g)
18% Al-Baseline	3092	3404	25.8	Al_2O_3	32.08	0.315
18% B	3008	2578	23.0	BN	11.31	0.456
18% Mg	2875	3255	24.4	MgO	12.96	0.322
18% Zr	2745	2983	26.8	ZrO_2	25.33	0.206
18% Mg10B90	2900	2558	23.7	BN	8.55	0.345
18% Mg15B85	2897	2546	23.9	BN	7.06	0.284
18% Mg20B80	2902	2531	24.1	BN	5.57	0.225
18% Mg25B75	2894	2514	24.4	BN	3.99	0.161
18% Mg60B40	2954	2845	24.5	MgO	8.83	0.219
15% Al + 3% Mg10B90b	3056	3238	25.5	Al_2O_3	26.00	0.255
15% Al + 3% Mg15B85a	3047	3248	25.3	Al_2O_3	26.12	0.256
15% Al + 3% Mg20B80a	3057	3255	25.6	Al_2O_3	26.27	0.258
15% Al + 3% Mg25B75a	3054	3261	25.6	Al_2O_3	26.45	0.259
15% Al + 3% Mg60B40b	3066	3316	25.9	Al_2O_3	22.86	0.224

Note: 1) CCP is Condensed Combustion Products; 2) In propellants loaded with Al, CCP consists of alumina Al_2O_3; 3) In propellants loaded with MgB, solid BN is present at the throat section, except propellant 15% Al + 3% Mg60B40; 4) For propellant 15% Al + 3% Mg60B40, CCP consists of MgO.

Despite these encouraging effects on condensed mass fraction, molar mass does not feature any dramatic modification. Therefore, the performance degradation due to lower adiabatic flame temperatures, because of different chemical and thermophysical properties of the ingredients, leads to lower ideal specific impulses in vacuum whenever Al is replaced. On the other hand, potential gains associated with the increase of specific impulse efficiency are attractive because the combined two-dimensional (2D) / two-phase (2P) flow effects promote substantial specific impulse losses, typically up to 2/3 of the total.[3] A quick look at the figures into play discourages a total Al replacement, while a partial replacement -say, of the order of 3% of Al (1/6 of the total Al load) - seems much more promising. For replacements such as nAl, this strategy works only if the CCP average size is properly reduced. For replacements such as Mg_xB_y, both the CCP fraction and average size can in principle be reduced.

Thus, in general, combining smaller CCP fraction and smaller agglomerate size may drive specific metallic additives to achieve a fruitful result by lowering 2P flow losses and exceed the specific impulse delivered by pure Al formulations. Such an idea needs a proper scrutiny to quantitatively assess all factors: while ideal thermochemistry is in principle enough to evaluate the produced CCP fraction for a given formulation, an appropriate experimental investigation is required to evaluate the average agglomerate size. It should be clear, however, that kinetic reasons may substantially affect the above global picture in either direction.

The objective of a given propulsive mission is accomplished by maximizing the velocity increment Δv imparted to the rocket vehicle by the well-known Tsiolkovsky equation

$$\Delta v = I_s \ln(1 + \rho V_p / M_f)$$

where ρ is the propellant density, V_p the propellant volume and M_f the final vehicle mass (initial vehicle mass-propellant mass). Therefore, the propellant density ρ may play an exceedingly important role and the use of denser energetic compounds, such as Titanium or Zirconium, becomes interesting. The less is the propellant mass fraction in the total launching mass, the higher is the propellant density input into the resulting Δv value. Thus, the density role increases for lower stages of launchers and other vehicles with relatively low ratio V_p / M_f (say, about $1.0 - 1.4$ L/kg).

The formulation Al (20% mass) + Hydrocarbon Binder (20% volume) + AP (balance), characterized by $I_s = 2462$ Ns/kg and $\rho = 1.85$ g · cm^{-3}, was taken as the reference baseline[18,19]. If this composition is replaced by another characterized by the values I_{s2} and ρ_2, one can calculate the so-called effective impulse (I_{ef}) of the second composition for the same vehicle. This means that, for a given ratio V_p / M_f, if Ief of the second composition is higher than 2462 Ns/kg, the replacement will augment Δv and will thus be more effective than the reference one; vice versa, if $I_{ef} < 2462$ Ns/kg, the formulation under investigation is less effective than the reference one. This comparison was carried out for several V_p / M_f values. At each V_p / M_f the effective impulse Ief was computed as

$$I_{ef} = 251 \ln(1 + 1.85 V_p / M_f) / \ln(1 + \rho_i V_p / M_f)$$

The generic ith composition, used in a vehicle with a given V_p / M_f ratio, achieves the same Δv value as any composition with $\rho = 1.85$ g · cm^{-3} and $I_s = I_{ef}$. In particular, the use of Zr or its hydride ZrH_2 (density 5.61 g · cm^{-3}) instead of Al in solid composite propellants may increase the ballistic effectiveness of the formulation because of the considerably higher propellant density notwithstanding the lower specific impulse (substantially lower than that of both Al and Mg); see Figure 2 for a typical trend. Replacing Al by Zr or ZrH_2 also allows the binder to grow up to 30% volume. The same composition achieves higher ballistic effectiveness if an active binder and a low oxygen excess oxidizer are used.

The maximum ballistic effectiveness, in compositions containing Zr or its hydride, is generally achieved when metal percentage is about $37\% - 46\%$, much higher than optimal Al content ($18\% - 22\%$). Both Zr and ZrH_2 are very flammable in powder form, and if used instead of Al allow to increase combustion rate too. Using Zr or ZrH_2 in a solid composite propellant offers the opportunity to choose between high ballistic effectiveness or, by increasing the binder fraction, better physical-mechanical properties.
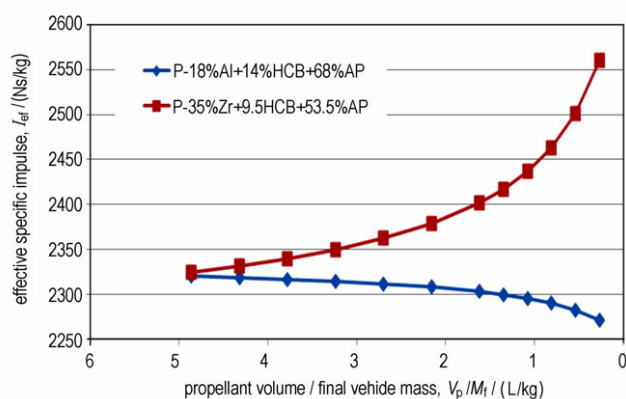
Fig. 2 Comparing the effective specific impulse for Zr- and Al-based formulations with inert binder.

3.2 Microstructure and Local Flame Temperature

Local flame temperature in the compound microstructure is computed assuming the pocket formulation discussed in Sec. 2.2.3. Only fine AP and HTPB are assumed to react in the pocket, producing a primary flame triggering a partial oxidation of the loaded metal (nAl, Mg_xB_y, etc.) and thus subsurface aggregation.

For propellants loaded with the Mg_xB_y composite metals, ideal thermochemistry of the microstructure was evaluated through the NASA CEA code over the pressure interval 5 to 25 bar and with a Mg coating ranging from 0 to 25%. Thermochemical analysis was performed neglecting the presence of Mg in the pocket since its low mass fraction has a negligible influence on final results under the assumption of nonreactive metal (less than 1 K for the temperature).

Local adiabatic flame temperature (T_{ad}) does not depend on the specific Al or Mg_xB_y powders as long as they behave as chemically inert ingredients; see Table 10. In the case of full combustion, metal powders release their chemical enthalpy and strongly raise the computed adiabatic flame temperature, depending on the enforced pressure and metal nature.

Table 10　Pocket adiabatic flame temperature for baseline and Mg_xB_y loaded propellants (as inert metals)

propellant	AP/%	HTPB/%	Al/%	B/%	T_{ad}/K at 5 bar	T_{ad}/K at 10 bar	T_{ad}/K at 20 bar	T_{ad}/K at 25 bar
18% Al-Baseline	23.81	33.33	42.86	0.00	983.33	1016.12	1050.02	1061.11
18% Mg_xB_y	23.81	33.33	36.43	6.43	981.65	1013.93	1047.22	1058.08

4　Combustion Experimental Results

　　The combustion features of the tested metallized solid propellants are compared to the standard Al-based ones in terms of steady burning rates, ignition, and agglomeration phenomena.

4.1　Steady State Burning Rate

　　The experimental rig used to measure steady state burning rates (r_b) is a windowed strand burner pressurized with N_2 or Ar. Propellant samples are sized $4 \times 4 \times 30$ mm, laterally inhibited and ignited by means of a hot wire. Chamber pressure is kept within a defined range by means of a controller and a set of servovalves. A video camera records the combustion allowing for digital post processing and regression rate measurement with a proprietary software. Burning rate data are then correlated with the Vieille's law. Three valid tests per pressure are used.

　　As an example, for the indicated B90-based dual-metal formulations, Figure 3 shows that the addition of Mg_xB_y composite metal powders leads to a measurable increase of steady burning rate with respect to the μAl-baseline, but not the pure B90-baseline. For the indicated B95-based formulations, Figure 4 shows that the addition of Mg_xB_y composite metal powders leads to an even more assessable increase of steady burning rate with respect to both the μAl -baseline and also the pure B95-baseline. In both cases, the precise content of Mg coating in the range 10% – 25% has a minor effect on the propellant regression rate. However, for increasing Mg content the burning rate gain vanishes; see for example the 60% Mg plot in Figure 4.

　　All of the steady state burning rates were deduced by analyzing the recorded videos with a dedicated software package and then fitted by a standard Vieille or Saint Robert law. Most tests were made in a N_2 atmosphere ranging from 1.5 to 40 bar. A summary of the fitted steady state burning rates in N_2, for many of the propellants studied in this work, is reported in Equations 1 – 14 hereafter. It is seen that the pressure sensitivity of Mg_xB_y formulations, evaluated by the ballistic exponent n of the Vieille-St. Robert law, is only slightly affected with respect to baseline ($n = 0.42$), with the exception of Mg60B40b ($n = 0.37$) and pure B ($n = 0.37$ for B90 and $n = 0.35$ for B95). On the contrary, P-18nAl 13d exhibits an increase of pressure sensitivity ($n = 0.52$).

$$r_b = (1.50 \pm 0.03) \cdot p^{(0.42 \pm 0.01)} \quad \text{reference-18Al} \quad \text{Equation 1}$$
$$r_b = (3.05 \pm 0.26) \cdot p^{(0.37 \pm 0.03)} \quad \text{P-18B90} \quad \text{Equation 2}$$
$$r_b = (2.84 \pm 0.22) \cdot p^{(0.35 \pm 0.03)} \quad \text{P-18B95} \quad \text{Equation 3}$$
$$r_b = (3.97 \pm 0.14) \cdot p^{(0.44 \pm 0.02)} \quad \text{P-18Mg15B85a} \quad \text{Equation 4}$$
$$r_b = (2.53 \pm 0.07) \cdot p^{(0.42 \pm 0.01)} \quad \text{P-3Mg15B85a} + \text{Al} \quad \text{Equation 5}$$
$$r_b = (3.99 \pm 0.13) \cdot p^{(0.43 \pm 0.02)} \quad \text{P-18Mg20B80a} \quad \text{Equation 6}$$
$$r_b = (2.68 \pm 0.05) \cdot p^{(0.39 \pm 0.01)} \quad \text{P-3Mg20B80a} + \text{Al} \quad \text{Equation 7}$$
$$r_b = (4.16 \pm 0.23) \cdot p^{(0.43 \pm 0.03)} \quad \text{P-18Mg25B75a} \quad \text{Equation 8}$$

$$r_b = (2.48 \pm 0.08) \cdot p^{(0.40 \pm 0.01)} \quad \text{P-3Mg25B75a} + \text{Al} \quad \text{Equation 9}$$
$$r_b = (4.45 \pm 0.23) \cdot p^{(0.44 \pm 0.02)} \quad \text{P-18Mg10B90b} \quad \text{Equation 10}$$
$$r_b = (3.07 \pm 0.05) \cdot p^{(0.41 \pm 0.01)} \quad \text{P-3Mg10B90b} + \text{Al} \quad \text{Equation 11}$$
$$r_b = (3.41 \pm 0.32) \cdot p^{(0.37 \pm 0.04)} \quad \text{P-18Mg60B40b} \quad \text{Equation 12}$$
$$r_b = (2.27 \pm 0.04) \cdot p^{(0.41 \pm 0.01)} \quad \text{P-3Mg60B40b} + \text{Al} \quad \text{Equation 13}$$
$$r_b = (1.61 \pm 0.03) \cdot p^{(0.52 \pm 0.01)} \quad \text{P-18nAl 13d} \quad \text{Equation 14}$$
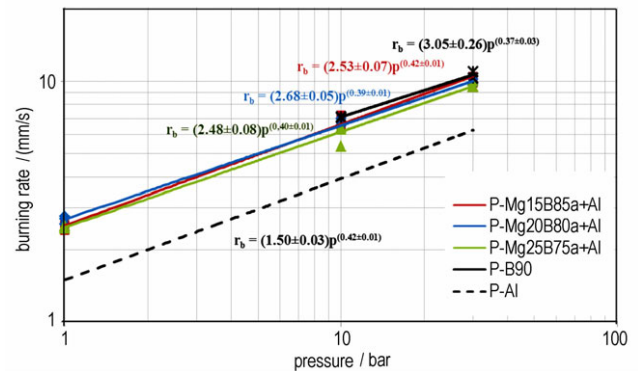
Fig. 3　Steady burning rates of B90-based dual-metal solid propellants: Mg_xB_y addition produces a measurable increase of burning rate with respect to the Al-baseline but not with respect to the B90-baseline, while the exact Mg content in the range 15% – 25% is not influential.
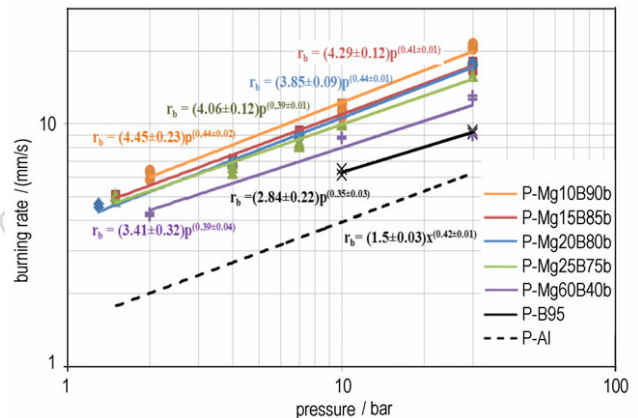
Fig. 4　Comparing steady burning rates of B95-based solid propellants: Mg_xB_y addition with 10% – 20% Mg coating produces a strong increase of burning rate with respect to both the Al-baseline and also B95-baseline, while a large fraction of Mg coating, for example 60%, is detrimental.

4.2　Aggregation/Agglomeration Phenomena

　　Tests to evaluate the agglomeration phenomena were performed under N_2 atmosphere at 5, 10, 20, and 25 bar; some experiments were repeated in Ar without noticeable changes. Combustion was performed in a strand burner, recorded by a high-resolution and high-speed video camera for slow motion post-processing and later analyzed with graphic

software. For each test, the incipient agglomerate size was manually measured for 200 particles as shown in Figure 5, and the d_{43} mean diameter was finally calculated. For all experimental tests, with the current optical setup the minimum diameter distinctly observable was around 30 μm. As an example, the results obtained for the indicated B90-based dual-metal formulations, assuming for convenience a linear dependence on pressure, are illustrated in Figure 6 and reported in Table 11, testifying a general decrease of the average agglomerate size especially for 25% Mg coating.
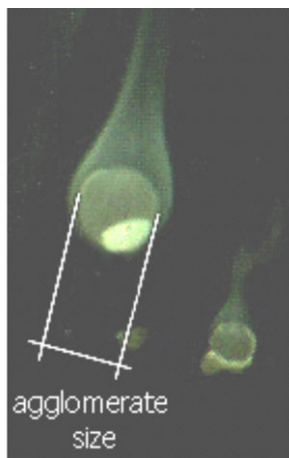
Fig.5 Example of manual measurement of incipient agglomerate size
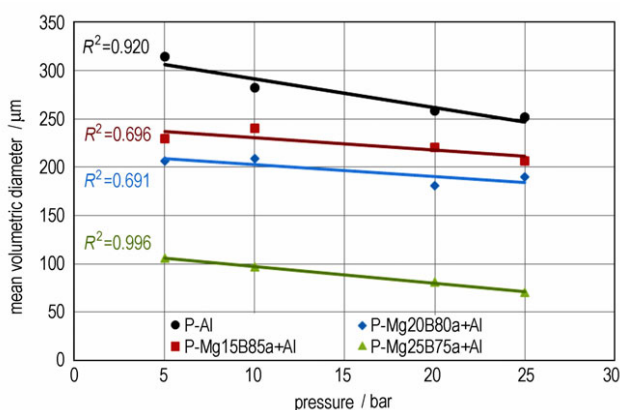
Fig.6 Average agglomerate size d_{43} vs. pressure of the indicated B90-based dual-metal solid propellants: Mg_xB_y addition with 15% − 25% Mg coating causes a general decrease of the average agglomerate size, especially for 25% Mg coating

Table 11 d_{43} mean diameters of incipient agglomerates for selected tested propellants   μm

propellants	pressure / bar			
	5	10	20	25
P-18Al baseline	315	282	259	252
P-3Mg15B85a + Al	229	240	221	206
P-3Mg20B80a + Al	206	209	181	190
P-3Mg25B75a + Al	106	97	81	70

Whereas all of the tested propellant formulations containing micrometric Al produce agglomerates (spherical drops of liquid metal and alumina in combustion with a distinct oxide cap), no clear agglomeration phenomena could be detected for propellant formulations containing only the B compounds under examination. Even if agglomeration occurs generating burning drops below the optical system resolution or outside the optical system field of view, the combustion process of B compounds is essentially characterized by the formation of thin flakes (sintered fractal aggregates in the description of Ref. 20).

For propellant microstructures using nAl or Mg_xB_y as metallic ingredients, visual inspections of the near burning surface region point to aggregation phenomena (prompt oxidation) without the transition to agglomeration. This effect is accompanied and probably augmented by the simultaneous large burning rates of the relevant formulations. In turn, both phenomena can be ascribed to the large BET surface of the metal fuel and its low ignition temperature. Heating is provided by the conductive thermal wave preceding the burning surface with the possible augmentation by exothermic reactions of the local premixed flame.

4.3 Metal Powder Ignition Temperature

Ignition temperature (T_{ign}) was evaluated through a dedicated experimental rig. Investigated powders were positioned on a metal plate heated up by a laser beam properly deflected through beam benders. The powder is not directly heated, but it is warmed through conduction from the holder plate. Temperature, laser radiation, and ignition were monitored by a multichannel oscilloscope. The powder ignition was promptly detected by a photodiode, while the ignition temperature was deduced through a microthermocouple. The oscilloscope was also able to trace the laser shutter opening time. All powders were tested in air at 1 or 5 bar for at least 5 times. Results were statistically managed as shown in Table 12. For all tested nAl powders, the ignition temperature (at most 875 K at 1 bar) turns out much lower than that of micrometric Al (at least 1150 K) thanks to their much larger BET surface (see Table 3 and Table 4).

Table 12 Tign for selected tested metallic powders

metal powder	T_{ign}/K (at 1 bar)	T_{ign}/K (at 5 bar)
nAl 01i	875 ±17	NAv
nAl 01h	865 ±15	NAv
nAl 07c	791 ±51	NAv
nAl 07d	823 ±48	NAv
nAl 13d	732 ±27	NAv
B90	1005 ±31	880 ±105
Mg15B85a	949 ±40	845 ±70
Mg20B80a	907 ±61	897 ±37
Mg25B75a	893 ±25	843 ±53
Mg10B90b	835 ±20	NAv
Mg15B85b	842 ±22	NAv
Mg25B75b	854 ±22	NAv
Mg60B40b	1023 ±69	NAv

Comparing ignition temperatures of the metal powders tested in Table 12 with the corresponding adiabatic flame temperature of the pocket at the same pressure (see examples in Table 10), keeping the metal load chemically inert, one observes that the propellant microstructure temperature can be

appreciably higher than that of the metal powder ignition. Local exothermicity is then sufficiently high to promote ignition of the metallic powders and induce at least a partial participation in the combustion process, thus increasing the pocket adiabatic flame temperature and favoring the generation of smaller agglomerates.

In this respect, Mg_xB_y powders with a high Mg content are characterized by a more vigorous combustion of B leading to a higher temperature of the incipient agglomerate region. This behavior is confirmed by experimental results indicating a progressive decrease of d_{43} with the increase of Mg content (see Figure 6). Therefore using Mg_xB_y as additive assures a strong reduction of agglomerate mean size with respect to the Al-baseline, up to 72% at 25 bar; see Figure 6.

5 Incipient Agglomeration as a Statistical Microstructure Effect

The process of CCP formation is the result of intermingled factors correlated to propellant composition and microstructure, as demonstrated by early works of Povinelli and Rosenstein[21] and more recently by Babuk[22]. As the loaded metal powder gets closer to the burning surface during combustion, it first interacts with the local propellant composition. In this respect, heterogeneity plays a fundamental role, because the propellant is a mixture of coarse and fine oxidizer particles, metal fuel, and binder matrix. As a consequence, the burning surface composition during combustion continues to evolve in both time and in space. In the search for an agglomeration model capable of accounting for the spatial nonhomogeneous displacement of ingredients, Cohen proposed a pioneering theoretical framework, called pocket model, where coarse oxidizer particles encapsulate fuel rich regions made by fine oxidizer, metal fuel, and binder[13]. Relying on this framework and extending the analysis to random microstructure, SPLab recently focused on a joint effort of modeling and experimental activities to elucidate more subtle microstructure and local chemistry effects.

Specifically, SPLab is investigating how agglomeration is connected to heterogeneity and pocket structure, and is trying to correlate statistical microstructure data from packing codes, burning rates, and mean agglomerate sizes[23,14,15,16]. A 2D routine for the generation of model combustion surfaces was implemented, along with a set of spatial statistical tools for the identification of mean pocket sizes. In particular, 2-Points Probability Functions were implemented giving the probability of finding 2 phases in the examined section, as a function of distance and angle; this allows the definition of the maximum probability of a phase exchange (that is, starting from a binder zone to find an AP zone and vice versa). The location of the maximum probability is considered to be representative of the pocket size, even though it does not coincide with its physical size. The pocket model framework suggests including metal, binder and possible fine AP ($5-10$ μm) in the so-called matrix phase, while medium and coarse AP grains compose the AP phase. Details of the sections creation and of the 2-Points Probability Functions calculation algorithms are fully discussed in references [23,24]. Examples of sections and 2-Points Probability Functions are reported in Figure 7.
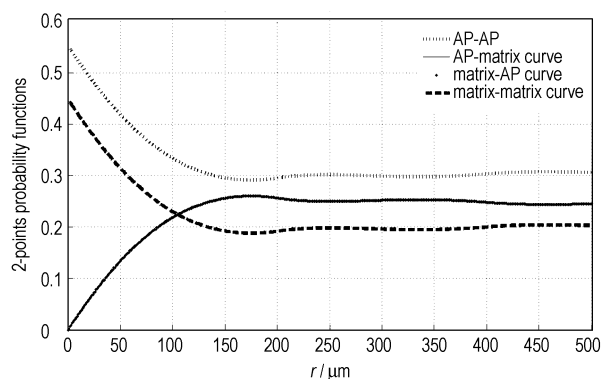
Fig. 7 Example of 2D section (up) and associated 2-Points Probability Functions (down). For symmetry reasons, AP-Matrix and Matrix-AP curves overlap.

This statistical approach allows defining of a characteristic length of the propellant microstructure as the location of the maximum probability of a phase exchange. However, the combustion of energetic materials implies that the microstructure has a limited life-time, which is the time available for the incipient metal aggregation in the pocket. This leads to the further definition of a characteristic time as twice the characteristic length divided by the steady burning rate. For a given propellant formulation, while the characteristic length depends solely on geometrical factors, the associated characteristic time is also a function of pressure through the propellant steady burning rate.

The microstructure characteristic length has proven[15,16] to fit adequately, almost linearly, the d_{43} mean diameters experimentally observed at the burning surface of a number of industrial solid propellants based on standard micrometric Al particles; see Figure 8. However, the expression obtained only partially reproduces the results for a laboratory replica of the reference propellants and fails to predict the aggregation effects observed for some specific metals. Overall, this statistical analysis demonstrated that a purely geometric approach for the prediction of agglomeration is not a universal tool, notwithstanding the fairly good results achieved for aluminized compositions. Burning rate and agglomerate residence time represent only two intermingled parameters out of a complex scenario. In fact, the pocket represents a region with its local chemical composition and reactivity. Surrounded by coarse

oxidizer particles, fuel vapors as well as small oxidizer decomposition products mix up promptly as in a premixed flame, by virtue of the small size of fine AP.
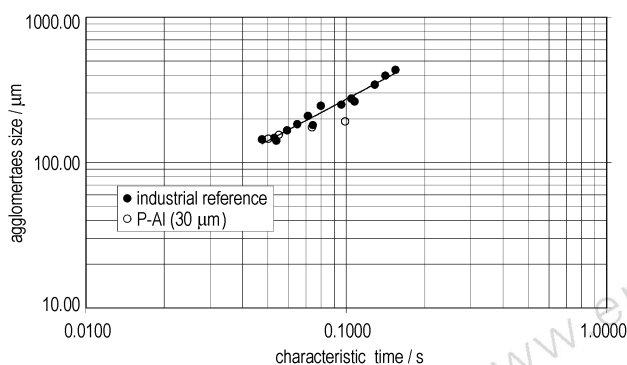
Fig. 8 Mean agglomerate size dependence on characteristic time for a-luminized propellants

Experimental analyses confirm the dependence of agglomeration on pocket flame properties. A series of lab-scale propellants, with the same nominal compositions, were produced varying the ratio between the fine and coarse fraction of AP. The fine AP content was changed in the range 0 to 40% as detailed in Table 13. Sizes of agglomerates generated during propellant combustion for pressures spanning from 5 to 30 bar were obtained through SPLab proprietary optical technique already depicted by Figure 5. Mass mean agglomerate sizes (d_{43}) as a function of fine AP mass fraction are reported in Figure 9 and correlated through spline and exponential fitting interpolations for maxima findings. As expected, the increase of pressure leads to smaller agglomerates for all propellants. On the other hand, if the combustion pressure is fixed, the reader can recognize a maximum for CCP size in the range 5% to 10% of fine AP fraction, with a decreasing trend with increasing pressure. Upper pressure limit is imposed by the optical analysis and does not allow assessment if this effect is disappearing for a specific combustion condition.

Table 13 Experimental propellants based on different AP fractions used for Figure 9

propellant label	AP coarse/%	AP fine/%	Al/%	HTPB/%
AP00	68	0	18	14
AP05	63	5	18	14
AP10	58	10	18	14
AP20	48	20	18	14
AP40	28	40	18	14

The observed behavior can be explained by the presence of two concurrent effects contributing to the size of aggregates/agglomerates inside the pocket. Burning rate sets the residence time of metal particles. With a fixed formulation, agglomerates are smaller as the propellant burns faster (high pressure). At the same time, fixing the combustion pressure, the local temperature in the pocket is correlated to propellant formulation, driven by the fine AP/HTPB mixture enclosed within the coarse AP surrounding structure. As a consequence, being the relevant temperatures close to the Al melting point, higher fractions of fine AP increase the local surface temperature,

thus leading to warmer metal on the surface, more prone to aggregation. However, higher fractions of fine AP increase burning rate, as well. The resulting trend is a compromise. For low fine AP fractions (5% to 10%), the regression rate increase does not overcome the effect of local temperature increase, thus favoring large agglomerate size. Details are reported in previous works.[25]
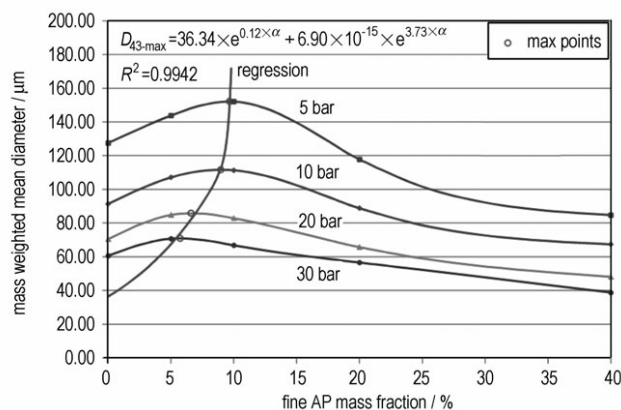
Fig. 9 Mass weighted mean diameters of CCP vs. fine AP mass fraction and best-fit exponential interpolation of maxima

6 Conclusions and Future Work

6.1 Metallized Solid Propellants

In general, an optimum exists of dual metal formulations (μAl-nAl and μAl-Mg$_x$B$_y$) leading to improved ballistic properties under real operating conditions. For μAl-Mg$_x$B$_y$ formulations, best results in terms of reduced average agglomerate size are obtained with 25% Mg coating, while 60% Mg coating leads to a measurable decrease of steady burning rate.

A basic role is played by the propellant microstructure. In agreement with previous findings[26], the intimate mixing with the surrounding decomposition products of the fine AP fractions and binder promotes the formation of partially oxidized and intermediate metallized thin flakes (prompt metal oxidation). The ignition temperature has been reported to be about 900 K for nAl[27,28], while for B it is estimated around 1900 K for single particles[25] and down to 1200 K for agglomerates[29]. The experimental data of Table 12 confirm the value of nAl and also point out the beneficial effect of Mg in lowering the Mg$_x$B$_y$ ignition temperature to the same level of nAl.

Depending on steady state burning rate (i.e., pressure), type of binder, fine oxidizer size and fraction, metal average size and distribution, unburned metal may also contribute to the thin flake formation. Peculiar effects shown in Figure 3 and Figure 9 confirm that not only geometry but also the chemistry and physics of the microstructure are important in controlling the propellant combustion and performance.

6.2 Future Work

For metallized formulations, full control of nano-sized ingredient dispersion and compound rheology is still an open issue. At any rate, dual-metal formulations is the recommended strategy to optimize performance and properly tailor ballistic as well as mechanical properties. Future work will

continue on optimization of the B compound, Al hydrides, and dual metal formulations for practical applications in rocket propulsion.

References：

[1] Price E W. Combustion of Metallized Propellants, Fundamentals of Solid Propellants Combustion [M]. edited by K K Kuo and M Summerfield, Vol. 90, Chapter 9, AIAA Progress in Aeronautics and Astronautics, 1984.

[2] Babuk V A, Vasilyev V A, Sviridov V V. Formation of Condensed Combustion Products at the Burning Surface of Solid Rocket Propellant, Solid Propellant Chemistry, Combustion, and Motor Interior Ballistics [M]. edited by V Yang, T B Brill, and W Z Ren, Progress in Astronautics and Aeronautics, AIAA, Reston, VA, 2000, pp. 749 −776.

[3] Reydellet D, et al. Performance of Rocket Motors with Metallized Propellants in AGARD Advisory Report AR-230. AGARD, Paris, France, 1986. AGARD PEP WG-17.

[4] Sarner S F. Propellant Chemistry, [M]. Reinhold Publishing Corporation, New York, NY, USA, 1966.

[5] Miller W H. Solid Rocket Motor Performance Analysis and Prediction, Technical Report NASA-SP-8039, NASA, 1971.

[6] Coats D E, et al. A Computer Program for the Prediction of Solid Propellant Rocket Motor Performance, Technical Report AFRPL-TR-75-36 Vol. I-III, Air Force Rocket Propulsion Laboratory, Edwards AFB, CA, USA, 1975.

[7] DeLuca L T, Galfetti L, Severini F, et al. Physical and Ballistic Characterization of AlH3-based Space Propellants[J]. *Aerosp Sci Technol*, 2007,11(1)：18 −25.

[8] DeLuca L T, Galfetti L. Burning of Metallized Composite Solid Rocket Propellants：from Micrometric to Nanometric Aluminum Size. [C]// Proc.. 3rd AJCPP, Gyeongju, Korea, 2008 .

[9] Babuk V A, Dolotkazin I, Gamsov A, et al. Nanoaluminum as a Solid Propellant Fuel [J]. *J Prop Power*, 2009, 25(2)：482 −489.

[10] DeLuca L T, Marchesi E, Spreafico M, et al. Agglomeration Effects in Metallized Solid Rocket Propellants ,Theory and Practice of Energetic Materials, Vol. VIII, Proceeding of IASPEP [M]. LI Shengcai, WANG Yajun, CAO Fengxia, ZHAO Shanshan, and ZHOU Shuqiong, Science Press, 2009, pp. 258 −270.

[11] DeLuca L T, Galfetti L, Colombo G, et al. Microstructure Effects in Aluminized Solid Rocket Propellants [J]. *J Prop Power*, 2010, 26：4, pp. 724 −33.

[12] Sossi A, Duranti E, Paravan C, et al. Coated nano-sized Aluminum powders：physical analyses and performance tests in hybrid propulsion [C]//4th EUCASS, St. Petersburg, Russia, 2011.

[13] Cohen N S. A Pocket Model for Aluminum Agglomeration in Composite Propellants[J]. *AIAA J*,1983, 21(5)：720 −725.

[14] Maggi F, Stafford S, Jackson T L, et al. Nature of Packs Used in Propellant Modeling [J]. *Physical Review*,2008, 77：1 −17.

[15] Maggi F, Bandera A, Galfetti L, et al. Efficient Solid Propulsion for Access to Space [J]. *Acta Astronaut*, 2010, 66：1563 −1573.

[16] Maggi F, Bandera A, DeLuca L T. Approaching Solid Propellant Heterogeneity for Agglomerate Size Prediction [C]//46th AIAA/ASME/ SAE/ASEE JPC & Exhibit, Nashville, TN, 25 −28 Jul 2010.

[17] S Gordon, B S McBride. Computer program for calculation of complex chemical equilibrium compositions and applications, Technical Report RP-1311, NASA Reference Publication, 1994.

[18] Lempert D B, Manelis G, Nechiporenko G. Superdense Zr-containing propellants with density higher than 2.1 kg/l [C]// XX AIDAA Congr. , Milan, Italy, June 2009.

[19] Brambilla M, Lempert D B, DeLuca L T. Ballistic effectiveness of Zr-containing Solid Composite Propellants as function of binder nature and mass fraction [C]// 4th EUCASS, Saint Petersburg, Russia, 2011.

[20] Chan M L, Parr T, Hanson-Parr D, et al. Characterization of a Boron Containing Propellant, IWCP Volume 9, Novel Energetic Materials and Applications[M]. L. T. DeLuca, L. Galfetti, and R. A. Pesce-Rodriguez, Paper 07. Grafiche GSS, Bergamo, Italy, 2004.

[21] Povinelli L A, Rosenstein R A. Alumina size distributions from high-pressure composite solid-propellant combustion [J]. *AIAA J*, 1964, 2(10)：1754 −1760.

[22] Babuk V A, Vasilyev V A, Malakhov M S. Condensed combustion products at the burning surface of aluminized solid propellant [J]. *J Prop Power*, 1999, 15(6)：783 −793.

[23] Bandera A. Combustion of Metallized Solid Rocket Propellants and Motor Performance[D]. PhD Thesis in Energetics, Politecnico di Milano, Milano, Italy, April 2009.

[24] Maggi F, Bandera A, DeLuca L T, et al. Agglomeration in Solid Rocket Propellants：Novel Experimental and Modeling Methods [J]. *Prog Prop Phys*, 2011, 2：81 −98.

[25] Maggi F, Dossi S, DeLuca L T. Agglomeration and pocket structures in composite solid rocket propellants [C]// 4th EUCASS, St. Petersburg, Russia, 2011.

[26] Mitani T, Izumikawat M. Combustion Efficiencies of Aluminum and Boron in Solid Propellants[J]. *J Spacecraft Rockets*, 1991, 28：1, pp. 79 −84.

[27] Beckstead M W. A Summary of Aluminum Combustion, NATO RTO EN 023, 2004.

[28] Trunov M A, et al. Ignition of Aluminum Powders Under Different Experimental Conditions [J]. *Propell Explos Pyrot*, 2005, 30 (1)：36 −43.

[29] Shevchuk V G, Zolotko A N, Polishchuk D I. Ignition of Packed Boron Particles[J]. *Combust Explo Shock*, 1975, 11：189 −192.